

Hot Deformation Behavior of Equiatomic FeCrNiMn High Entropy Alloy

Cai Zhen¹, Wu Tiandong^{2,3}, Wei Na^{2,3}, Mei Jinna¹, Xue Xiangyi^{2,3}

¹ Suzhou Nuclear Power Research Institute, Suzhou 215004, China; ² Xi'an CHAOJING Technology Co., Ltd, Xi'an 710200, China; ³ Shaanxi Key Laboratory of Advanced Metal Structural Materials Precision Thermoforming, Xi'an 710200, China

Abstract: The hot deformation behavior of the equiatomic FeCrNiMn high entropy alloy was studied through the isothermal compression at 900–1050 °C with strain rate of 0.001–1 s⁻¹. Results show that the initial microstructure is mainly composed of equiaxed grains with face-centered cubic structure and fine body-centered cubic phase particles. The flow curves exhibit the typical single stress peak type. The peak stress is decreased significantly with increasing the temperature and decreasing the strain rate. The constitutive model was developed based on the hyperbolic-sine law to predict the flow stress. The stress exponent and the apparent activation energy were calculated as 3.13 and 405 kJ/mol, respectively. The processing maps were obtained based on the dynamic material model at different strains. It is found that no instability zone appears in the processing maps at different strains, suggesting the excellent hot deformability of the alloy. The deformation microstructure is closely related to the power dissipation efficiency η . The recrystallization fraction is 17.6vol% when η is 28%, and it is increased to 37.5vol% when η is 38%. Two optimal hot working condition ranges can be identified according to the processing maps: 900–940 °C/strain rate of 10⁻³~10^{-1.3} s⁻¹ and 960–1050 °C/10⁻³~10^{-0.3} s⁻¹.

Key words: high entropy alloy; deformation behavior; flow curve; FeCrNiMn

In recent years, the high entropy alloys (HEAs) with excellent mechanical properties have been widely developed and attract much attention^[1-3]. HEA is usually composed of more than four elements with the equiatomic or near-equiatomic proportion (5mol%~35mol% of each element)^[4-6]. Traditionally, the additional phases can be formed with increasing the number of component elements. However, HEAs contain fewer phases, which indicates that the high mixing entropy can increase the compatibility among different components, therefore avoiding the generation of terminal solid solution or intermetallic compounds caused by the phase separation^[7]. The representative equiatomic HEA is FeCrNiMnCo alloy^[8]. Although the composition of FeCrNiMnCo alloy is complex, the alloy is simply composed of face-centered cubic (fcc) single phase. Many novel HEA families are proposed, including 3D transition HEAs, refractory HEAs, and light HEAs^[9-11]. Moreover, the alloy phases include not only the fcc phase, but also the body-centered cubic (bcc) phase, dual-phase, and even multiphases.

HEAs containing multi-principal elements exhibit superior properties, such as ultrahigh hardness, high strength, high ductility, excellent microstructural and mechanical stability at high temperatures, and exceptional wear, corrosion, and oxidation resistance^[12]. Therefore, HEAs present great potential in nuclear and aerospace industries^[13]. However, the multi-components usually result in the slow diffusion, thereby leading to the composition inhomogeneity and some defects during the traditional ingot metallurgy^[12], i. e., the HEAs are hard to process. Thus, the proper processing method and parameters are required to refine the microstructure and to homogenize the element distribution.

The hot deformation behavior of HEAs has been widely researched, and great progress has been achieved in the fields of deformation kinetics and deformation mechanism^[14-17]. However, due to the complicated composition, the deformation characteristics of HEAs are still in need of investigation. In this research, the deformation behavior of the equiatomic FeCrNiMn alloy was investigated through the

Received date: November 11, 2021

Foundation item: National Natural Science Foundation of China (51901019)

Corresponding author: Wei Na, Master, Engineer, Xi'an CHAOJING Technology Co., Ltd, Xi'an 710200, P. R. China, E-mail: weina@super-c.com.cn

Copyright © 2022, Northwest Institute for Nonferrous Metal Research. Published by Science Press. All rights reserved.

isothermal compression tests, and the flow characteristics were revealed based on the kinetics analysis. Furthermore, the processing parameters were identified based on the processing maps.

1 Experiment

The experiment alloy was composed of Fe, Cr, Ni, and Mn with the equal atomic ratio. After two times of the induction suspension melting, an ingot with the dimension of $\Phi 90$ mm \times 400 mm was prepared. Then, the ingot was annealed at 1200 °C for 1 h followed by air-cooling to reduce the chemical segregations. For isothermal compression, the specimens with the size of $\Phi 8$ mm \times 12 mm were machined from the ingot. The hot compression tests were conducted on the Thermecmaster-Z simulator at temperatures of 900, 950, 1000, and 1050 °C. The specimens were heated to target temperatures with the heating rate of 10 °C/s and held at target temperatures for 5 min for temperature homogenization. Then the specimens were compressed at the constant strain rates of 0.001, 0.01, 0.1, and 1 s⁻¹ with the true strain of 1. Lubricants were applied between the specimen and the anvils to decrease the friction. During the deformation, the true stress-true strain curves were instantaneously recorded. After compression, the specimens were sectioned and mechanically polished followed by electrolytic polishing for the microstructure observation. The microstructure was analyzed by the Zeiss-sigma500 scanning electron microscope (SEM) equipped with electron back-scattered diffraction (EBSD). X-ray diffraction (XRD) was conducted to determine the phases.

2 Results and Discussion

2.1 Initial microstructure

The microstructure of the HEA after annealing is shown in Fig. 1a. The yellow area represents the fcc phase and the red area represents the bcc phase. According to XRD pattern in Fig. 1b, it is also confirmed that both fcc and bcc phases exist in the alloy. Besides, according to Fig. 1a, the alloy mainly consists of equiaxed fcc grains with the mean size of 80 μ m. Many annealing twins can be observed inside the grains. Meanwhile, the bcc particles are distributed inside the fcc phase or along the grain boundaries. The bcc particles are small with the mean size of only 7 μ m.

2.2 Flow curve

The true stress-true strain curves of HEAs at different temperatures and strain rates are shown in Fig. 2. It can be noticed that the flow curves exhibit the typical single peak type, which is similar to those of the alloys with low stacking-fault energy^[18]. At the early stage of the deformation, the work hardening is obvious, so the stress is increased rapidly with increasing the strain. Meanwhile, the work hardening rate is continuously reduced with increasing the strain, leading to the presence of a broad stress peak of the flow curves. After that, the alloy continuously softens and finally reaches a steady state. According to the classic theories^[18], the presence of the single stress peak indicates that the dynamic recrystallization

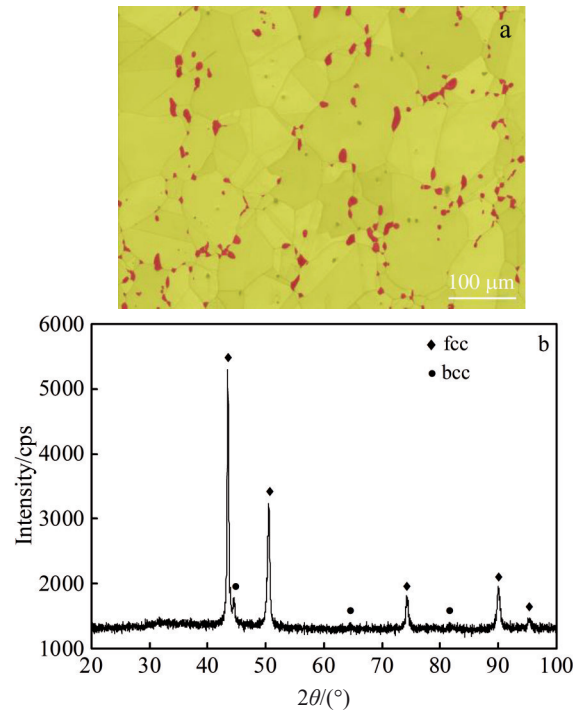


Fig.1 Microstructure (a) and XRD pattern (b) of initial HEA

(DRX) dominates the deformation instead of the dynamic recovery (DRV), owing to the low stacking-fault energy. Furthermore, the peak stress is quite sensitive to the temperature and strain rate. As shown in Fig. 3, with increasing the temperature and decreasing the strain rate, the peak stress is decreased significantly.

2.3 Deformation kinetics and constitutive modeling

In general, the hot deformation of metallic materials is a thermo-activated process, and the deformation kinetics can be well-described by the Arrhenius-type equations^[19,20], as follows:

$$\dot{\epsilon} \exp(Q/RT) = A\sigma^n \quad (1)$$

$$\dot{\epsilon} \exp(Q/RT) = A \exp(\beta\sigma) \quad (2)$$

$$\dot{\epsilon} \exp(Q/RT) = A [\sinh(\alpha\sigma)]^n \quad (3)$$

where A , α , and β are material constants; R is the gas constant (8.3154 J \cdot mol⁻¹ \cdot K⁻¹); $\dot{\epsilon}$ and σ are strain rate (s⁻¹) and flow stress (MPa), respectively; T is the deformation temperature (K); Q is the apparent activation energy (J/mol); n is the stress exponent.

In general, the power function equation Eq.(1) is suitable for hot deformation with low flow stress ($\alpha\sigma < 0.8$) and the exponential equation Eq.(2) is suitable for hot deformation with high flow stress ($\alpha\sigma > 1.2$). The hyperbolic-sine equation Eq.(3) is the combination of the abovementioned two equations and has a wide application. Because the compression tests in this research were conducted under a wide range of temperature and strain rate, Eq.(3) was applied to model the flow behavior of HEAs.

In order to determine the parameters, Eq.(1-3) can be reorganized into the following expressions:

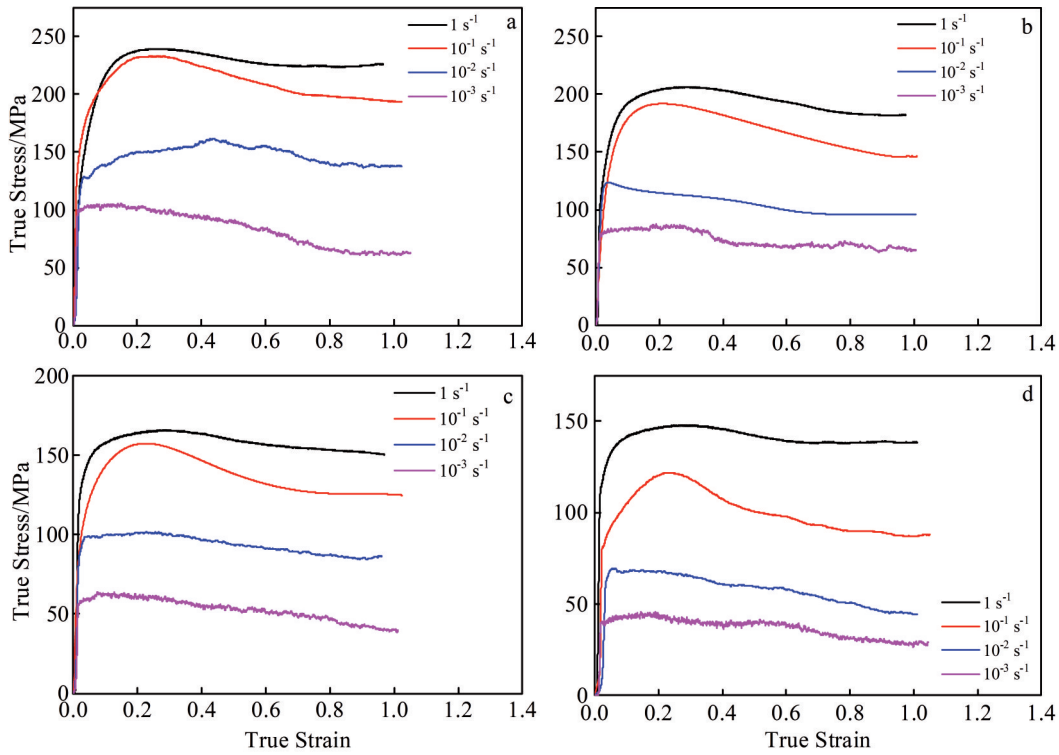


Fig.2 True stress-true strain curves of FeCrNiMn HEAs at different temperatures: (a) 900 °C; (b) 950 °C; (c) 1000 °C; (d) 1050 °C

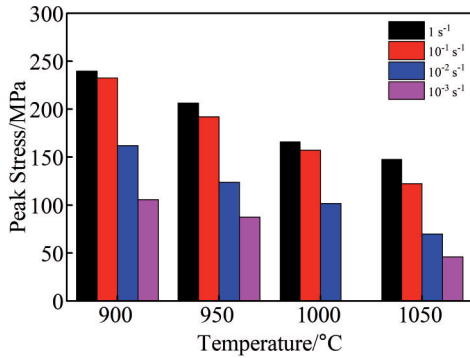


Fig.3 Effects of temperature and strain rate on peak stress of FeCrNiMn HEAs

$$\ln \dot{\epsilon} = \ln A + n \ln \sigma - Q/RT \quad (4)$$

$$\ln \dot{\epsilon} = \ln A + \beta \sigma - Q/RT \quad (5)$$

$$\ln \dot{\epsilon} = \ln A + n \ln [\sinh(\alpha \sigma)] - Q/RT \quad (6)$$

Based on the peak stress at different conditions, the values of n and β can be calculated by Eq. (4) and Eq. (5), respectively. Fig.4a and 4b show the relationships of $\ln \dot{\epsilon} - \ln \sigma$ and $\ln \dot{\epsilon} - \sigma$, respectively. Through the linear fitting, the n and β can be obtained from the slope of the fitting curves. Then the parameter α can be determined by $\alpha = \beta/n = 0.0083$. According to Eq.(6), the activation energy can be expressed by Eq.(7), as follows:

$$Q = R \left(\frac{\partial \ln \dot{\epsilon}}{\partial \ln [\sinh(\alpha \sigma)]} \right)_T \left(\frac{\partial \ln [\sinh(\alpha \sigma)]}{\partial (1/T)} \right)_\dot{\epsilon} \quad (7)$$

As shown in Fig.4c and 4d, through the linear regression

calculation, the mean Q value is obtained as about 405 kJ/mol. Finally, the corrected n value is obtained as 3.13, according to Fig. 4e (Zener-Hollomon parameter Z represents the temperature-compensated strain rate). In addition, it can be noticed that the correlation coefficient of the linear regression is 0.98, indicating that the hyperbolic-sine equation can accurately predict the flow stress, and the constitutive model can be expressed as follows:

$$\dot{\epsilon} = 7.72 \times 10^{14} [\sinh(0.0083\sigma)]^{3.13} \exp\left(-\frac{405000}{RT}\right) \quad (8)$$

According to the constitutive analysis, the studied HEA has a relatively high activation energy. In general, the deformation activation energy is close to the lattice diffusion energy of the alloys^[21]. The high activation energy may be caused by the slow diffusion in HEAs^[7]. However, this HEA also exhibits a low stress exponent, i. e., a high strain rate sensitivity (m), which indicates that the alloy has excellent hot deformability.

2.4 Processing maps and microstructure characteristics

The processing map can not only reflect the deformation mechanism at different strains, but also present the unstable zones, thereby providing references and optimization guidance for hot working^[22]. The processing map of FeCrNiMn HEA is based on the dynamic material model (DMM)^[23], which is related to the deformation mechanism with the dynamic response of the microstructure during hot deformation. According to the dissipative structure theory, the total energy (P) required per unit volume of material during hot deformation can be described as follows:

$$P = \sigma \dot{\epsilon} = G + J = \int_0^{\dot{\epsilon}} \sigma d\dot{\epsilon} + \int_0^{\sigma} \dot{\epsilon} d\sigma \quad (9)$$

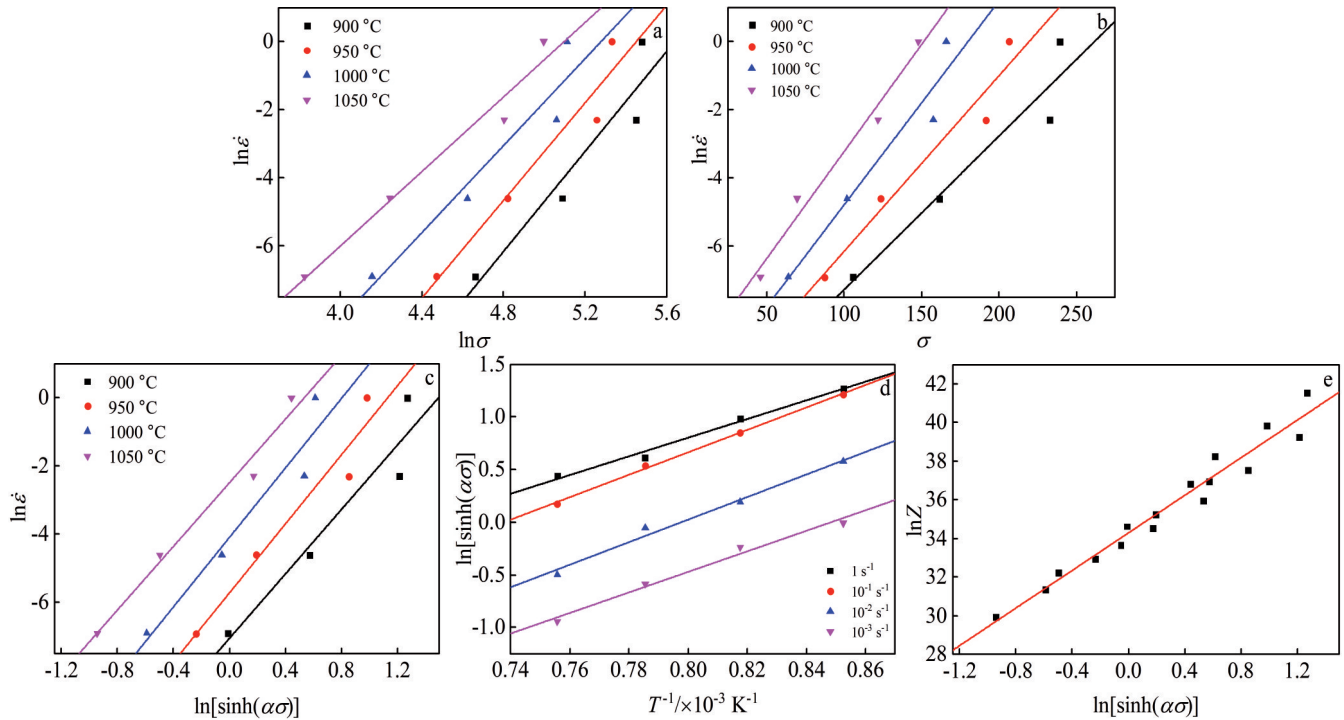


Fig.4 Relationships of $\ln \dot{\epsilon}$ - $\ln \sigma$ (a), $\ln \dot{\epsilon}$ - σ (b), $\ln \dot{\epsilon}$ - $\ln[\sinh(\alpha\sigma)]$ (c), $\ln[\sinh(\alpha\sigma)]$ - T^{-1} (d), and $\ln Z$ - $\ln[\sinh(\alpha\sigma)]$ (e)

where G is the deformation viscous heat and J is the power consumed by the microstructure evolution, such as recrystallization, recovery, and phase transformation^[23]. Meanwhile, the strain rate sensitivity m can be represented by Eq. (10), as follows:

$$m = \frac{dJ}{dG} = \frac{\dot{\epsilon} d\sigma}{\sigma d\dot{\epsilon}} = \frac{d \ln \sigma}{d \ln \dot{\epsilon}} \quad (10)$$

Assuming that the material is in the ideal linear dissipation state, then the maximum J value is obtained as follows:

$$J_{\max} = \frac{P}{2} = \frac{\sigma \dot{\epsilon}}{2} \quad (11)$$

The changes of power dissipation efficiency factor η with the deformation temperature and strain rate are shown in the power dissipation map and η can be expressed by Eq.(12), as follows:

$$\eta = \frac{J}{J_{\max}} = \frac{2m}{m+1} \quad (12)$$

The instability of material during the hot deformation can be represented by the dimensionless parameter ζ ^[21], as follows:

$$\zeta(\dot{\epsilon}) = \frac{\partial \ln\left(\frac{m}{m+1}\right)}{\partial \ln \dot{\epsilon}} + m \quad (13)$$

The changes of ζ with the deformation temperature and strain rate are presented in the instability map. $\zeta < 0$ indicates the unstable zone in the instability map, which reveals the deformation instability of the material, such as wedge cracking and adiabatic shear zone^[23].

Therefore, the calculation of m value at various conditions is crucial. Normally, the m calculation is conducted by the spline interpolation method^[14,15]. However, it is inapplicable when there are a few experiment data. For instance, the m

value in this research is negative at low temperature and high strain rate through the spline interpolation calculation. Obviously, this is inconsistent with the actual results. Therefore, a novel m calculation method under deformation conditions is proposed.

The rate-equation of equiatomic FeCrNiMn HEA can be expressed as follows:

$$\sigma = \frac{1}{\alpha} a \sinh\left(\frac{\dot{\epsilon}}{B}\right)^m \quad (14)$$

where B is a material constant without the consideration of temperature compensation. All the involved parameters can be obtained through the experiment data. Then the strain rate sensitivity m can be obtained based on Eq.(14).

By superimposing the power dissipation maps on the corresponding instability maps, the obtained processing maps at different strains are shown in Fig.5. It is noticeable that due to the positive ζ values at all conditions, there is no instability zone in the processing maps, demonstrating the excellent hot workability of the studied alloy. As for the power dissipation map, the higher the η value, the more the energy consumption by the microstructure conversion, and the better the hot workability of metallic materials when the η is greater than 30%^[24]. Accordingly, the individual processing maps can be divided into two domains, namely domain A with high η value and domain B with low η value.

As shown in Fig.5a, when the true strain is 0.2, the domain A contains the area with temperature $T=980\sim 1050$ °C and strain rate $\dot{\epsilon}=10^{-3}\sim 10^{-1} \text{ s}^{-1}$. The maximum η value of 36% is located at the point with the highest temperature and the lowest strain rate. With increasing the strain, the domain A expands towards the area with lower temperature and higher

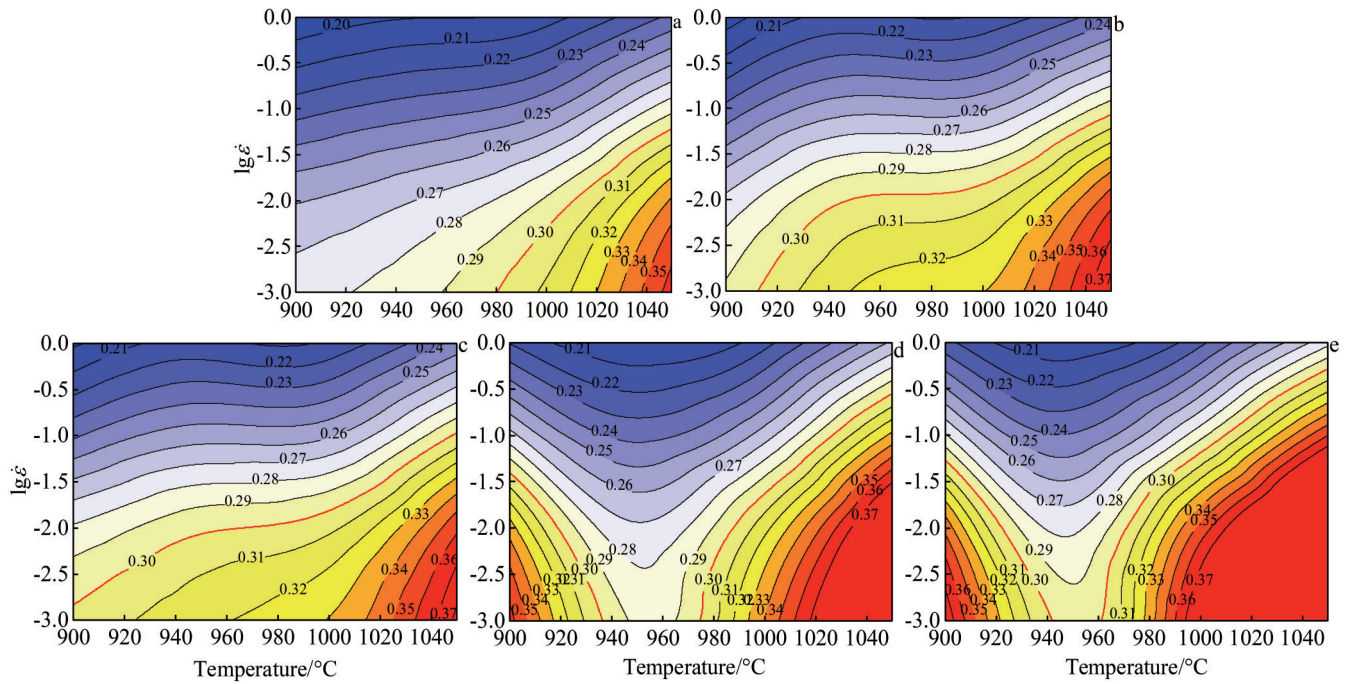


Fig.5 Processing maps of FeCrNiMn HEAs at strain of 0.2 (a), 0.4 (b), 0.6 (c), 0.8 (d), and 1.0 (e)

strain rate, as demonstrated in Fig.5b and 5c. However, when the strain increases to 0.8, the domain A splits into two parts, A_1 and A_2 . The temperature and strain rate in A_1 area are 900~936 °C and 10^{-3} ~ $10^{-1.4}$ s $^{-1}$, respectively; the temperature and strain rate in A_2 area are 974~1050 °C and 10^{-3} ~ $10^{-0.65}$ s $^{-1}$, respectively. This result implies that the hot workability of the HEA is significantly increased owing to the grain refinement.

Thus, with further increasing the strain to 1, the A_1 and A_2 areas are further increased.

Fig. 6 shows the HEA microstructures at 900 °C/1 s $^{-1}$ with $\eta=22\%$. The initial coarse fcc grains are evidently elongated, and the bcc particles are enlarged. A large amount of low angle grain boundary is formed inside the fcc grains, whereas the negligible DRX occurs at the grains boundaries. The bcc

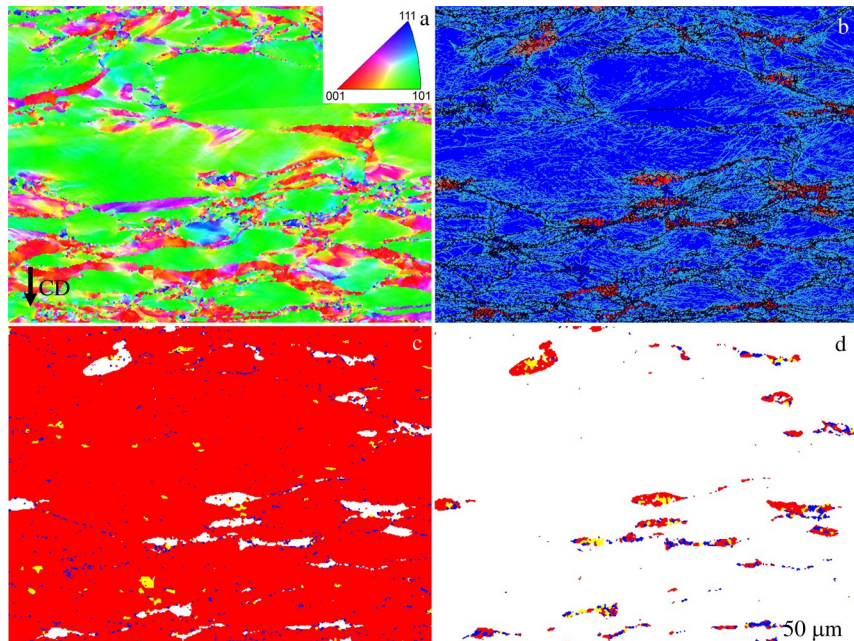


Fig.6 EBSD maps of FeCrNiMn HEAs deformed at 900 °C/1 s $^{-1}$: (a) inverse pole figure (CD is compression direction); (b) grain boundary distribution (black line is high angle grain boundary, green line is low angle grain boundary, blue area denotes fcc phase, and red area denotes bcc phase); (c) DRX fraction of fcc phase; (d) DRX fraction of bcc phase (red, yellow, and blue areas in Fig.6c and 6d represent deformed, substructured, and DRXed zones, respectively)

phase is also slightly DRXed. However, the area fraction of substructure is much larger than that of fcc phase, indicating different mechanical properties of the two components. In conclusion, when $\eta = 22\%$, slight DRX occurs in the FeCrNiMn HEA.

Fig. 7 shows EBSD analysis results of FeCrNiMn HEAs deformed at $950\text{ }^{\circ}\text{C}/10^{-2}\text{ s}^{-1}$ with $\eta = 28\%$ (the lower part of domain B). The fcc grains in matrix are severely elongated. The fine DRX grains can be observed at the grain boundaries, forming the necklace structure. However, there

is no DRX inside the grains and the extensive substructures are generated. The DRX fraction is about 17.6vol%, which is much higher than that under the condition of $\eta = 22\%$. In contrast, the bcc phases are completely fragmented, i.e., the bcc phases are DRXed. These bcc grains are mixed with DRXed fcc grains, which forms a micro-duplex structure along the fcc grain boundaries. Therefore, a slight increase of η to 28% can cause the noticeable DRX of the alloy.

As shown in Fig. 8, after the HEA is deformed at $1050\text{ }^{\circ}\text{C}/$

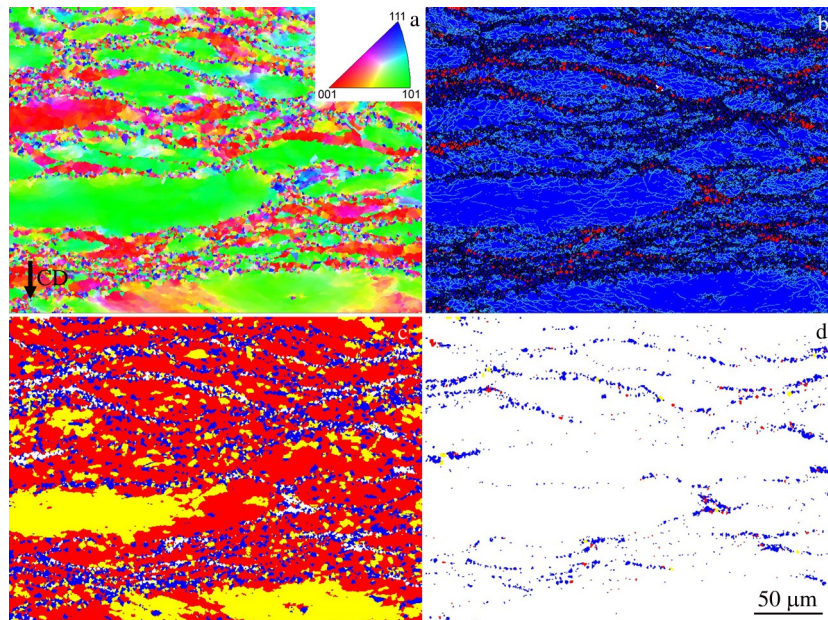


Fig.7 EBSD maps of FeCrNiMn HEAs deformed at $950\text{ }^{\circ}\text{C}/0.01\text{ s}^{-1}$: (a) inverse pole figure; (b) grain boundary distribution; (c) DRX fraction of fcc phase; (d) DRX fraction of bcc phase

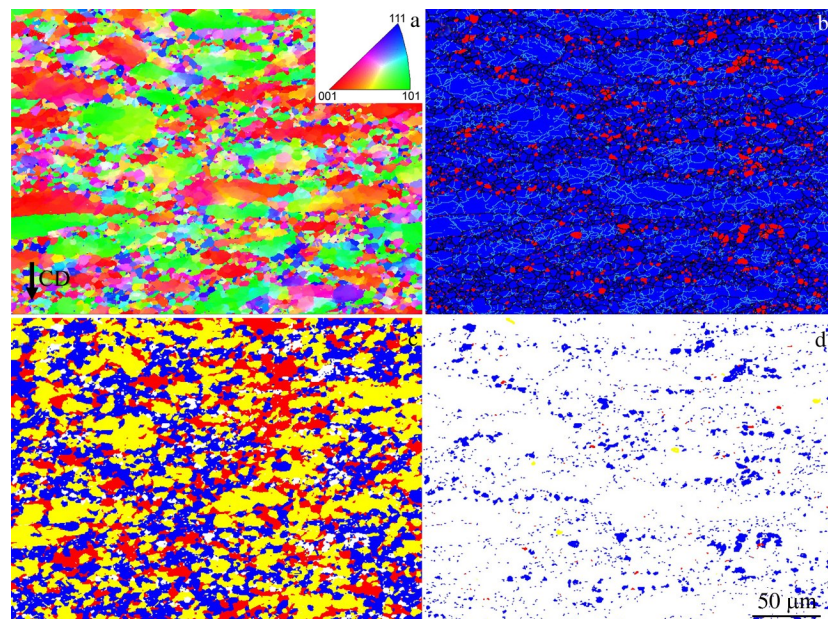


Fig.8 EBSD maps of FeCrNiMn HEAs deformed at $1050\text{ }^{\circ}\text{C}/0.001\text{ s}^{-1}$: (a) inverse pole figure; (b) grain boundary distribution; (c) DRX fraction of fcc phase; (d) DRX fraction of bcc phase

0.001 s⁻¹, the η rises to 38%. The DRX region continuously expands into the grain matrix, leading to the increase of DRX fraction to 37.5vol%. Meanwhile, most of the matrix contains substructures instead of deformed structures, indicating the intensive DRV inside the grains. The bcc phases are fully DRXed, and their distribution is much more homogeneous than that in Fig.7. This may be caused by the redistribution of the small grains due to the grain boundary sliding/rotation.

According to these analyses, it can be concluded that the studied HEA has excellent hot-workability, and no instability zone exists in the processing maps of the alloy. Meanwhile, the fragmentation of the initial microstructure is closely related to the dissipation efficiency factor. In order to achieve the maximum degree of microstructure conversion, the suitable processing conditions should be temperature $T=900\sim 942$ °C with strain rate $\dot{\epsilon}=10^{-3}\sim 10^{-1}$ s⁻¹ and $T=960\sim 1050$ °C with $\dot{\epsilon}=10^{-3}\sim 10^{-0.3}$ s⁻¹, i. e., the suitable condition can lead to the highest η .

3 Conclusions

1) The flow curves of the FeCrNiMn alloy exhibit the typical single stress peak type. The peak stress is significantly affected by the temperature and strain rate. With increasing the temperature and decreasing the strain rate, the peak stress is decreased dramatically.

2) The stress exponent (n) and activation energy (Q) are 3.13 and 405 kJ/mol, respectively. The low stress exponent indicates the superior hot-workability of the alloy. Moreover, a novel constitutive model is developed based on the hyperbolic-sine equation, which can accurately predict the flow stress.

3) Due to the superior hot workability, no instability region exists in the processing maps. The fragmentation fraction is positively related to the dissipation efficiency factor. Two suitable processing conditions are identified: temperature $T=900\sim 942$ °C with strain rate $\dot{\epsilon}=10^{-3}\sim 10^{-1}$ s⁻¹ and $T=960\sim 1050$ °C with $\dot{\epsilon}=10^{-3}\sim 10^{-0.3}$ s⁻¹, i. e., the suitable condition can lead to the highest power dissipation efficiency η .

References

- Zhang Y, Zuo T T, Tang Z et al. *Progress in Materials Science* [J], 2014, 61: 1
- Li Tianxin, Jiao Wenna, Miao Junwei et al. *Materials Science and Engineering A*[J], 2021, 827: 142 0661
- Li Tianxin, Lu Yiping, Cao Zhiqiang et al. *Acta Metallurgica Sinica*[J], 2021, 57(1): 42 (in Chinese)
- Yeh J W, Chen S K, Lin S J et al. *Advanced Engineering Materials*[J], 2004, 6(5): 299
- Otto F, Yang Y, Bei H et al. *Acta Mater*[J], 2013, 61(7): 2628
- Li Tianxin, Lu Yiping, Wang Tongmin et al. *Applied Physics Letters*[J], 2021, 119(7): 71 905
- Miracle D B, Senkov O N. *Acta Mater*[J], 2017, 122: 448
- Cantor B, Chang I T H, Knight P et al. *Materials Science and Engineering A*[J], 2004, 375: 213
- Lu Yidi, Zhang Xiaoyong, Hou Shuo et al. *Rare Metal Materials and Engineering*[J], 2021, 50(1): 333 (in Chinese)
- Zhao Haichao, Qiao Yulin, Liang Xiubing et al. *Rare Metal Materials and Engineering*[J], 2020, 49(4): 1457 (in Chinese)
- Li Yanchao, Li Laiping, Gao Xuanqiao et al. *Rare Metal Materials and Engineering*[J], 2020, 49(12): 4365 (in Chinese)
- Moghaddam A O, Shaburova N A, Samodurova M N et al. *Journal of Materials Science & Technology*[J], 2021, 77: 131
- Ye Y F, Wang Q, Lu J et al. *Materials Today*[J], 2016, 19(6): 349
- Jeong H T, Park H K, Park K et al. *Materials Science and Engineering A*[J], 2019, 756: 528
- Nayan N, Singh G, Murty S V S N et al. *Intermetallics*[J], 2014, 55: 145
- Rahul M R, Samal S, Venugopal S et al. *Journal of Alloys and Compounds*[J], 2018, 749: 1115
- Zhang Y, Li J S, Wang J et al. *Journal of Alloys and Compounds* [J], 2018, 757: 39
- Sakai T, Belyakov A, Kaibyshev R et al. *Progress in Materials Science*[J], 2014, 60: 130
- Sellars C M, McTegart W J. *Acta Meta*[J], 1966, 14(9): 1136
- McQueen H J, Ryan N D. *Materials Science and Engineering A* [J], 2002, 322(1-2): 43
- Cheng Liang, Li Jinshan, Xue Xiangyi et al. *Materials Science and Engineering A*[J], 2016, 678: 389
- Li H Y, Wei D D, Hu J D et al. *Computational Materials Science* [J], 5 2012, 53(1): 425
- Prasad Y V R K, Gegel H L, Doraivelu S M et al. *Metallurgical Transactions A*[J], 1984, 15(11): 1883
- Mcqueen H J, Yue S, Ryan N D et al. *Journal of Materials Processing Technology*[J], 1995, 53(1): 293

等原子比FeCrMnNi高熵合金的热变形行为

蔡 振¹, 吴天栋^{2,3}, 卫 娜^{2,3}, 梅金娜¹, 薛祥义^{2,3}

(1. 苏州热工研究院有限公司, 江苏 苏州 215004)

(2. 西安超晶科技有限公司, 陕西 西安 710200)

(3. 陕西省先进金属结构材料精确热成形重点实验室, 陕西 西安 710200)

摘 要: 采用等温压缩实验, 对FeCrNiMn等原子比高熵合金在900~1050 °C和0.001~1 s⁻¹区间内的热变形行为进行了研究。结果表明, 合金的初始组织主要由等轴面心立方晶粒和细小体心立方相颗粒构成。合金的流变曲线呈现典型的单峰形, 随着温度的提高和应变速率的降低, 峰值应力显著下降。基于双曲正弦方程建立了预测流变应力的本构模型, 同时计算了合金的应力指数和表观变形激活能, 分别为3.13和405 kJ/mol。基于动态材料模型建立了合金在不同应变量下的热加工图, 发现所有热加工图中均未出现变形失稳区, 说明合金具有优异的变形能力。通过与变形组织的对比发现, 变形组织与能量耗散因子值密切相关。当能量耗散因子值为28%时, 再结晶体积分数仅为17.6%; 当能量耗散因子值为38%时, 再结晶体积分数则提高至37.5%。通过热加工图确定了合金的2个最佳热变形参数区间: 900~940 °C/10⁻³~10^{-1.3} s⁻¹和960~1050 °C/10⁻³~10^{-0.3} s⁻¹。

关键词: 高熵合金; 变形行为; 流变曲线; FeCrMnNi

作者简介: 蔡 振, 男, 1991年生, 工程师, 苏州热工研究院有限公司, 江苏 苏州 215004, E-mail: p196526@cgnpc.com.cn